Role of core losses in drift-vortex interactions

E. Westerhof, J. Rem, and T. J. Schep
FOM-Instituut voor Plasmafysica ''Rijnhuizen,'' Association EURATOM-FOM, Postbus 1207, 3430 BE Nieuwegein, The Netherlands
(Received 24 February 1997)

Dipole drift vortices in the Hasegawa-Mima-Charney equation are studied by means of particle-in-cell (PIC) calculations. Apart from providing an efficient and accurate solution of the equations, PIC provides additional information about the fluid flow such as exchange of fluid between regions interior and exterior to the dipoles. Several cases of perturbed dipoles are studied with particular emphasis on the evolution of the fluid that is initially trapped inside the separatrix of the co-moving stream function of each unperturbed dipole. In particular, the effect of a finite tilt of the dipole axis is analyzed. Here, asymmetric losses from the two dipole halves are found to play a crucial role in the qualitative evolution of the dipole trajectory: dipoles initially moving in the unstable direction are found to reverse their average velocity perpendicular to the density gradient. Very large perturbations are obtained in dipole collisions. Here symmetry of the initial conditions plays an important role: collisions of aligned dipoles appear almost solitonlike, while for nonaligned dipoles the collision at least generates a tilt of the axes of the dipoles, but may also lead to a complete destruction of one of the poles. In all cases a significant loss of initially trapped fluid is demonstrated. [S1063-651X(97)14207-6]

PACS number(s): 52.35.Kt, 47.32.Cc, 52.65.−y

I. INTRODUCTION

A characteristic feature of two-dimensional (2D) fluid and plasma turbulence is the emergence of long-lived coherent structures through self-organization processes [1–3]. These coherent structures often take the form of large scale monopolar and dipolar vortices, and play an important role in the global transport of particles and energy [4]. Often the nonlinear fluid or plasma equations admit analytical solutions in the form of (dipole) vortices. The study of these solutions provides further insight into the behavior of vortices and their importance in turbulent transport. The Hasegawa-Mima-Charney (HMC) equation describes the 2D nonlinear evolution of electrostatic drift modes and turbulence in an inhomogeneous plasma with a uniform magnetic field. When the magnetic field is taken along the z axis and the density inhomogeneity $n_0(x)$, which gives rise to a constant drift velocity $v_* \equiv -(cT_e/eB)[d\ln n_0(x)/dx]$, is taken in the x direction, the HMC equation for the electrostatic potential ϕ can be written as [5,6]

$$\frac{\partial}{\partial t}(\phi - \nabla^2\phi + v_* x) + [\phi, \phi - \nabla^2\phi + v_* x] = 0, \qquad (1)$$

where time is normalized to Ω_{ci}^{-1}, lengths to the ion gyroradius at the electron temperature, and the potential to e/T_e. The Poisson bracket $[f,g] \equiv (\partial f/\partial x)(\partial g/\partial y) - (\partial f/\partial y)(\partial g/\partial x)$ is used to write the convection with the $\boldsymbol{E}\times\boldsymbol{B}$ drift as $[\phi,\cdot]$. The same equation describes the behavior of Rossby waves in a rotating atmosphere in the so-called beta-plane approximation (see, e.g., [6] for a detailed comparison). Equation (1) reflects the conservation of generalized potential vorticity $\overline{\omega} = \phi - \nabla^2\phi + v_* x$. Dipole solutions of the HMC equation have been obtained by Larichev and Reznik [7], and a large number of analytical and numerical studies of these dipoles, their stability and interaction, have been carried out (see, e.g., Refs. [8–13], or for a review see [6]). The dipoles propagate along the y axis perpendicular to the density gradient and their propagation velocity is restricted to the range $u < -v_*$, or $u > 0$, which is outside the range of phase velocities for linear drift waves.

We present a study of Larichev-Reznik dipoles by means of a particle-in-cell (PIC) code employing periodic boundary conditions. As shown by Eq. (1), the HMC equation is ideally suited for such an approach (cf. [14,15]). For example, the global conservation of generalized potential vorticity is inherent in the PIC algorithm. Other important conservation laws are those for energy, $E \equiv \frac{1}{2}\int[\phi^2 + (\nabla\phi)^2]dx\,dy$ and generalized ''enstrophy,'' $U \equiv \frac{1}{2}\int(\phi - \nabla^2\phi)^2 dx\,dy$. Also these are found to be well respected by the numerics. Most important for the results presented in this paper is that the particles provide fluid tracers, which contain a wealth of information for the interpretation of the dipole dynamics and fluid flows. In particular, it will be shown that perturbations of a dipole lead to significant exchange between the fluid trapped inside the separatrix of the co-moving stream function and the surrounding fluid. As most or all vorticity associated with the dipole is concentrated in this originally trapped fluid, this inevitably leads to a weakening of the dipole. In one set of calculations, the effect of a finite tilt of the dipole axis has been analyzed. Such a tilt is known to lead to a stable oscillatory trajectory for dipoles with positive y velocity, while for dipoles with negative y velocity the tilt is unstable [8,16]. Here, it is shown that an asymmetry in the losses from the two dipole halves is found to play a crucial role in the qualitative evolution of the dipole trajectory: dipoles initially moving in a direction subject to the tilt instability [16] are found to reverse their average velocity perpendicular to the density gradient towards the stable direction.

Very large perturbations may occur in dipole collisions. Even though in the case of perfect alignment of the dipole axes these collisions may appear almost solitonlike [8], our calculations again show the importance of detrapping of sizable fractions of trapped fluid from the original dipoles. Here

 © 1997 The American Physical Society

also the symmetry introduced by the alignment of the dipoles is crucial. The effect of breaking this symmetry is shown by a set of calculations for increasing misalignment (or ''impact parameter''). Again the advantages of PIC simulations are illustrated by the ability to trace the whereabouts after the collision of all fluid that was originally trapped by the dipoles.

This paper is organized as follows. A brief description of the numerical code is given in Sec. II. The results of numerical calculations are presented in Sec. III. Initial conditions for the calculations are obtained from the analytical dipole solutions of Ref. [7], or a superposition of these. Though these are not exact solutions on a periodic domain, consequent errors are found to be small, as the dipole fields decay exponentially at large distances. A first set of examples is presented in Sec. III A, in which a single dipole is perturbed by a finite tilt of its initial direction of propagation, resulting in a stable or unstable oscillation of the dipole trajectory depending on its initial direction of propagation [8,16,17]. A second set of simulations, presented in Sec. III B, has been performed for a dipole collision similar to that treated in Ref. [8], but with a varying ''impact parameter.'' Depending on the impact parameter, large differences in dipole dynamics are observed. The main conclusions from our work are summarized in Sec. IV.

II. PIC CODE FOR THE HASEGAWA-MIMA-CHARNEY EQUATION

In a PIC code, the Hasegawa-Mima-Charney fluid equation is solved by discretizing the fluid in the form of a large number of fluid parcels or quasiparticles. Each of the fluid parcels is assigned a given amount of generalized potential vorticity, which is conserved by the flow. The solution of the fluid equation is then achieved by moving the fluid parcels according to the flow that is calculated on a regular spatial grid on the basis of the $\overline{\omega}$ vorticity distribution obtained by interpolation from the fluid parcels to the grid. Here, each grid cell contains a large number of fluid parcels, and the stream function is effectively calculated in a mean-field approximation where nearest neighbor interactions are not accounted for. Thus, subgrid scale fluctuations are averaged out, which can be regarded as a form of numerical dissipation. In this procedure the fluid parcels are considered as point particles; i.e., deformations of the fluid parcels in the flow, such as stretching, are not accounted for.

In the code a two-dimensional (x,y) rectangular domain is taken with periodic boundary conditions. The grid in both x and y is regular and the particles are initially distributed homogeneously over the grid. As the flow is incompressible the particle distribution is expected to remain (close to) homogeneous, which is indeed verified by the code results apart from statistical fluctuations due to the finite number of particles per grid cell. The code then consists of the following basic procedures.

(a) Assignment of generalized potential vorticity from the particles to the grid. This is achieved by the triangular shaped cloud (TSC) algorithm [15]. This interpolation scheme leads to an effective suppression of the particle noise in the simulations, with a smoothing of the vorticity field only on the order of the grid cell size. Higher order interpolation kernels, as suggested for PIC calculations in Ref. [18], have been tried, but yielded a smoothing of the vorticity field over too large distances without any significant further reduction of the particle noise.

(b) Solution of the stream function ϕ. Once the generalized potential vorticity is known on the grid, the Helmholtz equation for the stream function,

$$\phi-\nabla^2\phi=\overline{\omega}-v_*x, \tag{2}$$

is solved. In the code the solution for ϕ is obtained by the Fourier transform method [19].

(c) Calculation of the particle velocities. First, a velocity field is calculated on the grid by central differencing of the stream function. Next, the velocity at the position of each particle is obtained by simple bilinear interpolation within a grid cell.

(d) The actual time stepping. Here a leap-frog-type algorithm is employed to achieve sufficient numerical accuracy and stability. The algorithm consists of the tracking of two generations of particles, one at odd and one at even time steps. The velocity with which the particles are advanced from time t_n to t_{n+2} is then based on the particle position, vorticity distribution, and corresponding stream function at time t_{n+1}. Initialization of the particles at t_{-1} is achieved along the lines described in Ref. [20], except that the stream function in all cases is obtained numerically as described above.

One complication arises in the leap-frog time stepping scheme, since the positions of the odd and even time particles are directly coupled only at the time of initialization. As time progresses in the simulation, trajectories of particles from odd and even time generations diverge due to numerical errors. When this divergence becomes too large, the calculation of the particle velocities (being based on the position of the corresponding particle from the other generation) is no longer accurate. In order to suppress this source of numerical error, particles from the odd-time generation are reinitialized on the basis of the even-time particles after a given number of time steps (typically 100–1000).

Typical grid sizes for the calculations presented below are 64×64 or 128×128 with 25 particles per grid cell. Energy conservation is found to be satisfied in all runs to within 1%. Enstrophy conservation is typically satisfied within 2% except for periods of very strong dipole interactions where losses of up to 5% are found. The latter can be explained by a transfer of enstrophy to sub-grid scales during such periods: the sub-grid scale fluctuations in $\overline{\omega}$ vorticity are smoothed out by the assignment to the grid, which results in a loss of enstrophy. For a limited number of cases, a final check on the numerical accuracy of the results has been performed either by increasing the number of particles per grid cell or by increasing the spatial resolution. The latter has been achieved by increasing the number of grid cells while keeping the number of particles per cell fixed and, thus, increasing the total number of particles as well. The increased accuracy did not lead to significant differences between the results.

III. NUMERICAL RESULTS

The HMC equation (1) is known to possess dipole vortex solutions. Analytical expressions for such solutions have been given by Larichev and Reznik [7]. These are obtained

by searching for stationary propagating solutions with velocity u in the y direction, i.e., solutions depending only on the combination $y-ut$, and thus by solving

$$[\phi-ux,\phi-\nabla^2\phi+v_*x]=0. \tag{3}$$

The Poisson bracket vanishes identically when the two arguments are functionally related by some arbitrary function F. The Larichev-Reznik dipole solution is obtained by taking for F a simple linear relation, with different coefficients inside and outside a given copropagating circle of radius r_0. The solutions in the inner and outer regions are then matched at the boundary. The solution that is obtained can be written as [7,21]

$$\phi=\begin{cases} u\left(\dfrac{r_0K_1(\rho r)}{K_1(\rho r_0)}\right)\cos\theta & \text{outer region } r>r_0 \\ u\dfrac{\rho^2}{\lambda^2}\left[\left(1+\dfrac{\lambda^2}{\rho^2}\right)r-\dfrac{r_0J_1(\lambda r)}{J_1(\lambda r_0)}\right]\cos\theta & \text{inner region } r\leqslant r_0, \end{cases} \tag{4}$$

where $\rho^2=1+v_*/u$ and the matching of the inner and outer solutions provides a dispersion relation for λ [7]:

$$\lambda r_0J_1(\lambda r_0)/J_2(\lambda r_0)=-\rho r_0K_1(\rho r_0)/K_2(\rho r_0). \tag{5}$$

Note that the requirement for real ρ limits the solutions to propagating velocities $u<-v_*$ or $u>0$, which means that precisely the range corresponding to phase velocities for the linear waves is excluded. In geophysical terms, positive u corresponds to eastward and negative u to westward propagation. In the comoving frame, the stream function possesses a separatrix at $r=r_0$: the fluid inside this separatrix is trapped and simply carried along with the dipole motion.

The initial conditions used in the numerical simulations presented below are based on these analytical dipole solutions or a superposition of two of them. Since the analytical solutions are obtained on an infinite domain, whereas periodic boundary conditions on a finite rectangular domain are applied in the numerics, they are not the exact solutions for the latter case. However, the error this introduces in the numerics is small, especially because of the exponential decay of the solution for large r. The same remark applies to the superposition of two analytical solutions: provided they are initially well separated so that the effect of the large r contribution of the one on the other is negligible.

A. Dipole stability

The dipoles in the HMC equation show a remarkable stability to all kinds of perturbations. Any attempt at an analytical proof of their stability, however, has failed [22]. Moreover, a small tilt of the axis of a dipole with $u<-v_*$ (westward) leads to an instability in the sense that the tilt will increase [8,16]. Perturbation of the dipole axis of a dipole with $u>0$ (eastward) only leads to a stable oscillation around the original straight trajectory [8,16]. However, a basic question is whether, or to what extent, the dipole as such stays intact along its orbit. Even modest losses of fluid and vorticity can lead, when integrated over long times, to large and qualitative changes in the dipole orbit. The different behaviors of the dipoles with negative and positive velocity can be explained by simple arguments based on the conservation of generalized potential vorticity [8,16]: a dipole will move in the direction of its axis; as the axis is tilted it will be displaced in x and the conservation of generalized potential vorticity will cause an imbalance in the vorticities of the two dipole halves; this imbalance causes the dipole axis to rotate; for positive velocity dipoles this rotation of the axis reduces the tilt, giving rise to a stable oscillation of the trajectory, whereas for negative velocity dipoles this rotation increases the tilt. In the latter case the dipole would be expected to follow a cycloidal or figure-eight-like orbit [8]. This behavior is also described well by a modulated singular point vortex approximation [23].

Analytical expressions for the period and amplitude of the oscillation of tilted positive velocity dipoles are given by Nycander and Isichenko in Ref. [16]:

$$T=\frac{4}{u}\left(\frac{P_d}{v_*S}\right)^{1/2}K[|\sin(\delta\theta/2)|], \tag{6}$$

$$\Delta x=2\sin(\delta\theta/2)\left(\frac{P_d}{v_*S}\right)^{1/2}, \tag{7}$$

where K is a complete elliptic integral of the first kind, $\delta\theta$ is the tilt of the axis of the dipole, $\boldsymbol{P}_d\equiv\int(\phi-\nabla^2\phi)\boldsymbol{r}dx\,dy$ is the vorticity dipole moment, and S the surface under the initial separatrix of the dipole vortex, $S=\pi r_0^2$. For negative u the period (or frequency) is found to become imaginary, indicating the growth of the instability [16].

We present here the results of two calculations for dipoles whose axes initially are tilted by 45° with respect to the y axis. This is achieved by changing $\cos\theta\rightarrow\cos(\theta+\delta\theta)$ with $\delta\theta=\pi/4$ in the Larichev-Reznik solution used as initial condition for the numerical calculations. In both cases the background drift velocity is chosen as $v_*=0.4$ and the dipole radius as $r_0=0.5$. The initial velocities are $u=0.5$ and -2.0. The results will be shown in terms of the orbits of the ''centers of vorticity'' of each of the poles. These centers of vorticity are defined by

$$\boldsymbol{r}_C\equiv\frac{\Sigma_i\overline{\omega_i\boldsymbol{r}_i}}{\Sigma_i\overline{\omega_i}} \quad \text{with} \quad r_i(t=0)\in\mathbb{C}, \tag{8}$$

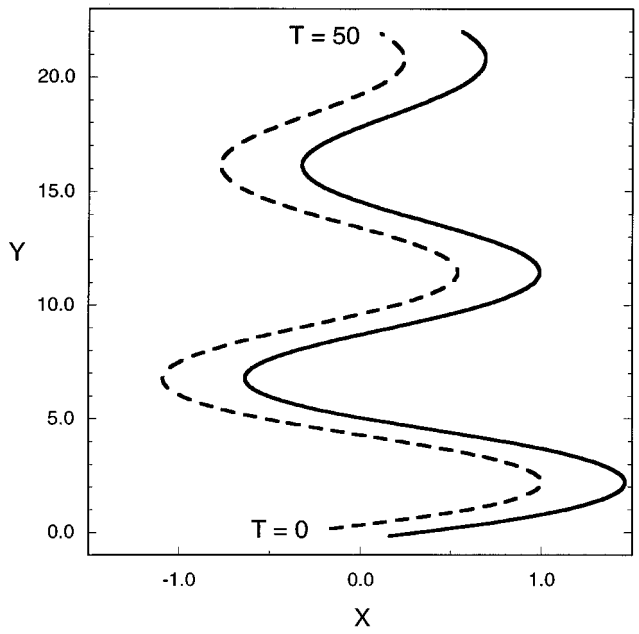

FIG. 1. Trajectories of the centers of vorticity of the halves (full line, $\overline{\omega}$ positive; dashed line, $\overline{\omega}$ negative) of a dipole tilted by 45° and with velocity $u=0.5$ (eastward), radius $r_0=0.5$, and drift $v_*=0.4$.

where the summation is over all particles i that at $t=0$ are trapped within the dipole half $\mathbb{C}$. With this definition one note of caution must be made: when a significant part of the initially trapped particles is lost from the dipole, the centers of vorticity will no longer give a good representation of the true position of each of the dipole halves. The calculated orbits of the centers of vorticity of the two dipole halves are presented in Figs. 1 and 2. The dipole with positive velocity (eastward)

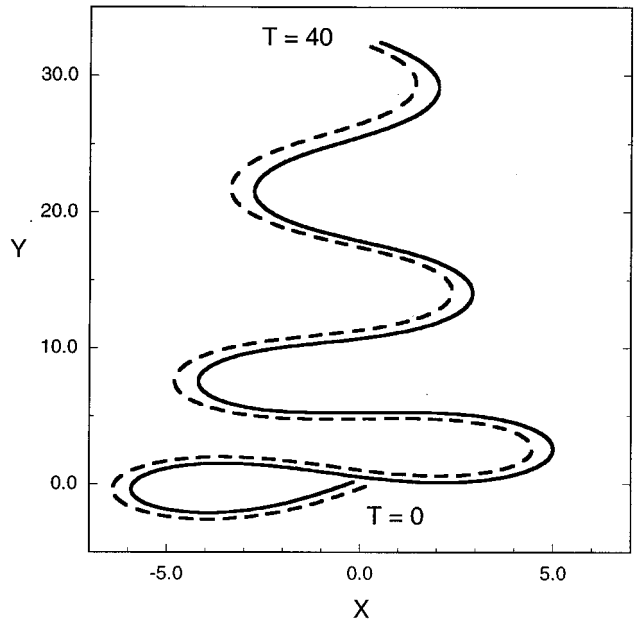

FIG. 2. Trajectories of the centers of vorticity of the halves (full line, $\overline{\omega}$ positive; dashed line, $\overline{\omega}$ negative) of a dipole tilted by 45° and with velocity $u=-2.0$ (westward), radius $r_0=0.5$, and drift $v_*=0.4$.

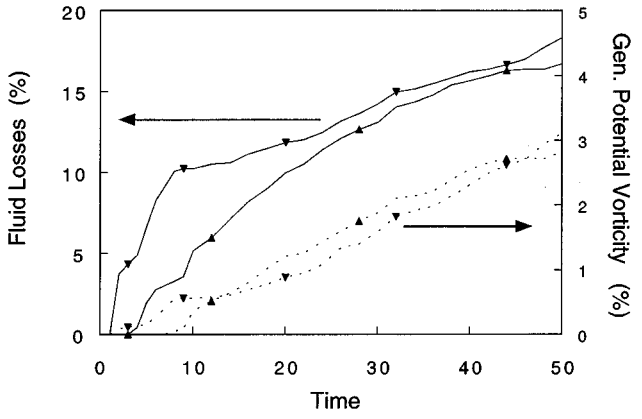

FIG. 3. Losses of fluid (full curves) and generalized potential vorticity (dashed curves) from each of the dipole halves of a stably tilted, positive velocity dipole (parameters as in Fig. 1). Curves marked by upward pointing triangles refer to the positive $\overline{\omega}$ pole, while downward pointing triangles refer to the negative pole.

is indeed seen in Fig. 1 to travel along a stable, oscillating trajectory. Substituting the appropriate values in the expressions (6) and (7) from Ref. [16], the period and oscillation are predicted to be $T=23$ and $\Delta x=1.4$, very close to the results of the numerical calculations, which yield $T=22$ and $\Delta x=1.2$, respectively. Similar results confirming the analytical predictions regarding period and amplitude of these oscillation are presented by Hesthaven *et al.* [17]. As can be clearly seen in Fig. 1, however, the oscillation is damped. This damping of the oscillation is a consequence both of a decrease in the dipole moment P_d, as well as of a small increase in dipole area S. The decrease in P_d is due to two effects: losses of originally trapped fluid, and mixing of fluid between the two dipole halves. Although fluid losses are compensated by trapping of ambient fluid, the latter has much lower $\overline{\omega}$ vorticity, such that the net result is a loss of vorticity. The loss of trapped fluid is a consequence of the breathing of the separatrices of the comoving stream function as the vorticity in each of the dipole halves changes due to the displacement in x [24,16]. The present PIC calculations provide a straightforward quantification of this loss of fluid or ''particles'' and of generalized potential vorticity. As can be seen in Fig. 3, the shedding of fluid and vorticity initially occurs in bursts at different times for the two dipole halves. After one cycle in its oscillation at $T=22$, the dipole has shed about 10% of the fluid that was inside its original separatrix. This fluid accounts for only about 1% of the generalized potential vorticity originally inside each of the dipole halves. This shedding of vorticity thus forms only part of the explanation of the damping of the oscillation. In addition, similar amounts of fluid are mixed between the dipole halves.

The trajectory of the negative velocity (westward) dipole indeed reflects the instability (i.e., the tilt initially increases). As is seen in Fig. 2, the first part of the orbit appears to be cycloidal as expected, but already before half a cycle is performed, the dipole reverses its average motion eastward, moving along a stable, damped oscillatory trajectory. Similar results are found for much smaller initial tilts as well. In conclusion, the tilt perturbation divides the dipoles into a

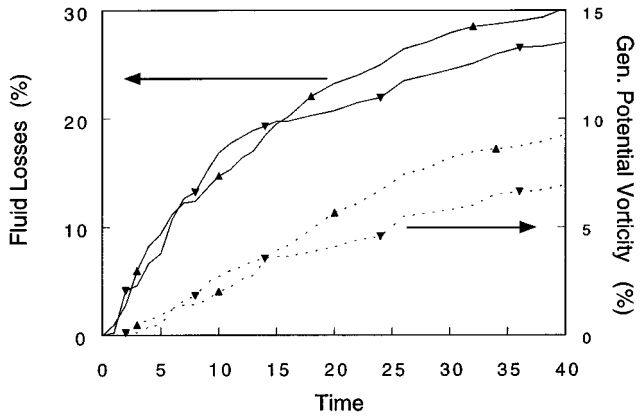

FIG. 4. Same as Fig. 3 for the unstably tilted, negative velocity dipole with the parameters of Fig. 2.

stable $u>0$ and a unstable branch $u<-v_*$, where the net result of the instability is a transition from the unstable towards the stable branch.

In order to understand how this change in the dipole trajectory comes about, we have performed calculations with a singular point-vortex model similar to those of Ref. [23], but with specified *ad hoc* vorticity losses from the two poles. The dipole orbit is reproduced well by the point-vortex model when a loss rate of generalized potential vorticity of about 0.5% per time unit is assumed, where for parts of the orbit with $x<0$ the loss is limited to the positive pole and with $x>0$ it is limited to the negative pole. This asymmetric loss of vorticity results in the qualitative change of the dipole orbit. Without any loss of generalized potential vorticity, the dipole would cross $x=0$ with the same velocity as it had initially, except that the velocity in the x direction has changed sign. In the first half of the cycloidal orbit the vorticity losses are limited to the positive pole, which at negative x is the pole with the larger vorticity. This results in a smaller imbalance between the two poles and, consequently, a slower rotation rate of the dipole axis, with the result that $x=0$ is crossed with a smaller velocity in the y direction. Eventually the net result is a reversal of the average y velocity.

The asymmetry in the loss of generalized potential vorticity, which is required to explain the dipole orbit, is not reflected in the losses of initially trapped fluid and the related vorticity losses as shown in Fig. 4. However, the fluid losses must necessarily be compensated by the entrainment of ambient fluid, which itself carries generalized potential vorticity equal to the background potential vorticity $\overline{\omega}\approx v_* x$. From this entrainment of ambient fluid the asymmetry in the vorticity losses can now be understood: at $x<0$ the newly trapped fluid has negative potential vorticity and, consequently, enhances the vorticity losses of the positive pole, but compensates the losses of the negative pole; the opposite holds for $x>0$.

B. Dipole collisions

The PIC calculations also provide more insight into the dynamics of dipole vortex collisions. In head-on collisions with zero impact parameter the dipole vortices show a remarkable robustness: in a calculation by Makino *et al.* [8] the dipole vortices appear to emerge almost unchanged after the collision. The dipole vortices are said to behave almost solitonlike. As will be shown below, this conclusion is only partly true.

Figure 5(a) shows the orbits of the centers of vorticity of each of the dipole halves during the zero impact parameter collision with identical parameters as in Ref. [8]: drift velocity $v_*=0.1$, dipole radii $r_0=0.5$, velocities $u_1=+0.3$ and $u_2=-0.5$, initial positions $x_{1,2}=0.0$, $y_{1,2}=\mp 1.5$. In this and all following pictures the orbit and particles initially associated with each dipole half are colored green and yellow for the stronger, negative velocity dipole and red and blue for the weaker, positive velocity dipole. The red and green colors correspond to the positive $\overline{\omega}$ poles and the blue and yellow colors to the negative $\overline{\omega}$ poles. At the collision the original dipoles split. The halves of the different dipoles then form unbalanced dipoles that travel along symmetric, near circular orbits. In the process, the weaker blue and red dipole halves are pulled around the stronger green and yellow halves. After a half circle, a second collision occurs in which the original dipoles reform. When looking at level curves of the vorticity or potential, the two dipoles appear almost unaffected by the collision, in which respect our calculations agree well with those of Ref. [8]. This is clearly not the case when one considers Fig. 5(b), which gives the final, $t=13$, positions of all particles initially trapped inside the separatrix of the comoving stream function of each dipole half. Clearly, both dipoles have lost a significant part of their initially trapped fluid. In order to estimate these losses, those particles are counted that are by visual inspection no longer associated with their original dipole. In this way, we can conclude that the weaker, blue-red dipole has exchanged 25% of its fluid with the ambient medium, a small part of which is trapped by the other dipole. For the stronger, green-yellow dipole, still 14% of its trapped fluid is exchanged with the ambient medium or the other dipole. Because of the strong concentration of the vorticity near the cores of the vortex poles, however, the exchanged fluid accounts for only 4.2% and 1.2%, respectively, of the generalized vorticities in each dipole half. This important effect of the collision will be missed by considering only level curves of vorticity or potential. The halves of the weaker, blue-red dipole also appear to have separated slightly, which together with the small loss of vorticity has resulted in a 13% lower velocity. The velocity of the stronger, green-yellow dipole has decreased by only 2%.

The solitonlike behavior is typical only of the special symmetric case of aligned dipoles: i.e., with zero impact parameter $b\equiv|\Delta x/r_0|=0$, where Δx is the distance between the axes of the dipoles. Various authors have performed calculations for collisions with nonzero impact parameter and noted the much stronger and possibly even destructive interaction of the dipoles in such cases. Here, we present a scan in impact parameter while keeping all other parameters fixed to those of Ref. [8] (see also above). With the impact parameter increasing as $b=0.2$, 0.4, 0.6, 0.8, and 1.0, respectively, Figs. 6–10 show the orbits of the centers of vorticity for the four dipole halves during the collision and the distribution shortly after the collision of fluid particles initially inside each of the dipole halves. In some cases the red dipole half is

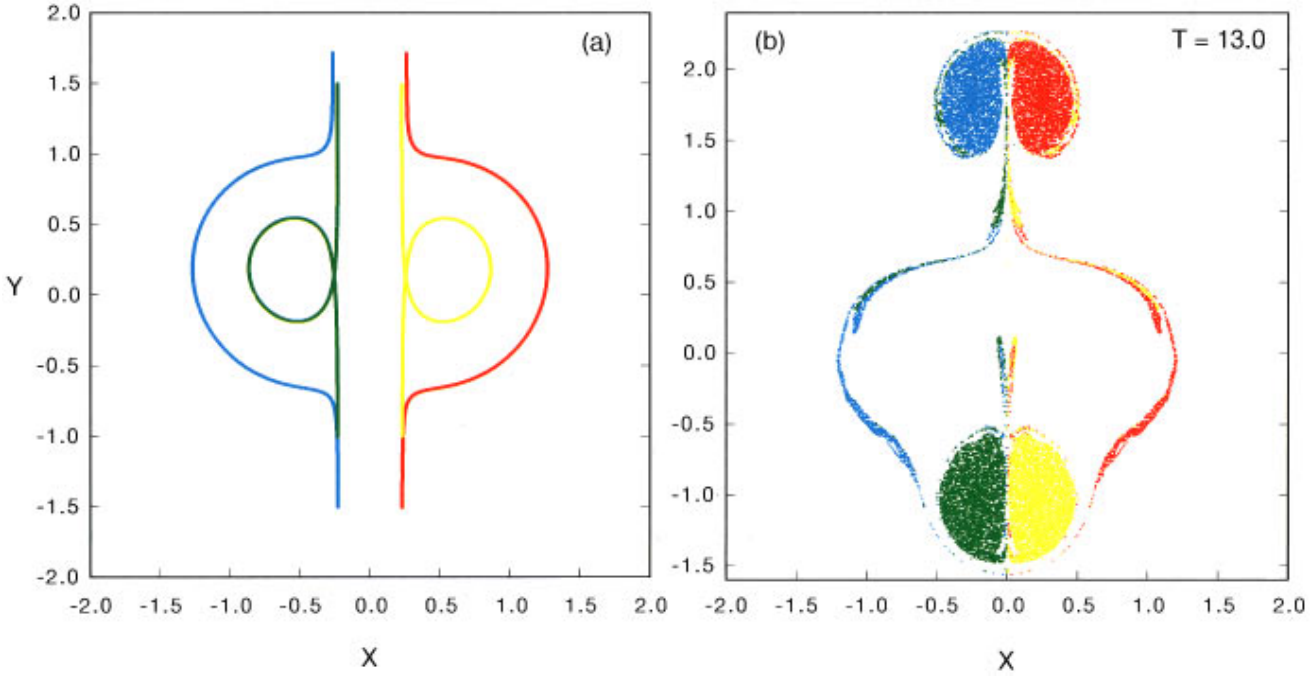

FIG. 5. (Color.) (a) Orbits of the centers of vorticity during a zero impact parameter collision of two aligned dipoles. (b) The positions at $T=13$ after the collision of fluid particles that in the initial conditions are trapped by the four poles, i.e., those particles that initially lie within the separatrices of the comoving stream functions of each of the dipoles. The parameters are as in Ref. [8]: drift velocity $v_*=0.1$, dipole radii $r_0=0.5$, velocities $u_1=+0.3$ for the red-blue dipole and $u_2=-0.5$ for the yellow-green dipole, with initial positions $x_{1,2}=0.0$, $y_{1,2}=\mp 1.5$. Red and green represent the positive $\overline{\omega}$ poles and blue and yellow the negative poles.

almost completely destroyed or broken into several pieces. In those cases the red center of vorticity loses its meaning as an indicator of the position of that pole, and is no longer drawn.

As the impact parameter is increased from zero, at first the two dipoles survive still largely intact. For small impact parameter, the asymmetric initial conditions result also in asymmetric final conditions in the sense that after the reforming collision both dipoles emerge with their axes tilted with respect to the y axis. As a consequence, the negative velocity, green-yellow dipole will become subject to the tilt instability described above. With increasing impact parameter the impact parameter of the second, reforming collision

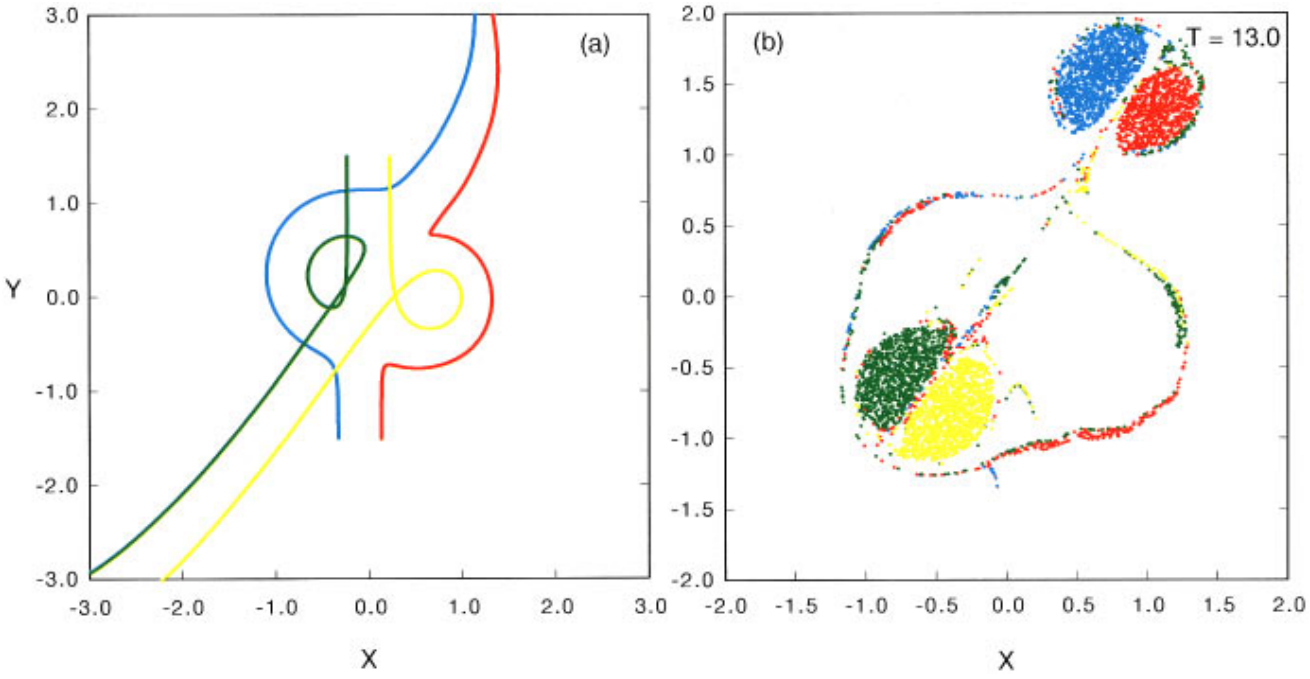

FIG. 6. (Color.) Same as Fig. 5, but for a finite impact parameter $b=0.2$. Only the initial position x_1 of the red-blue dipole has been changed to $x_1=-0.1$.

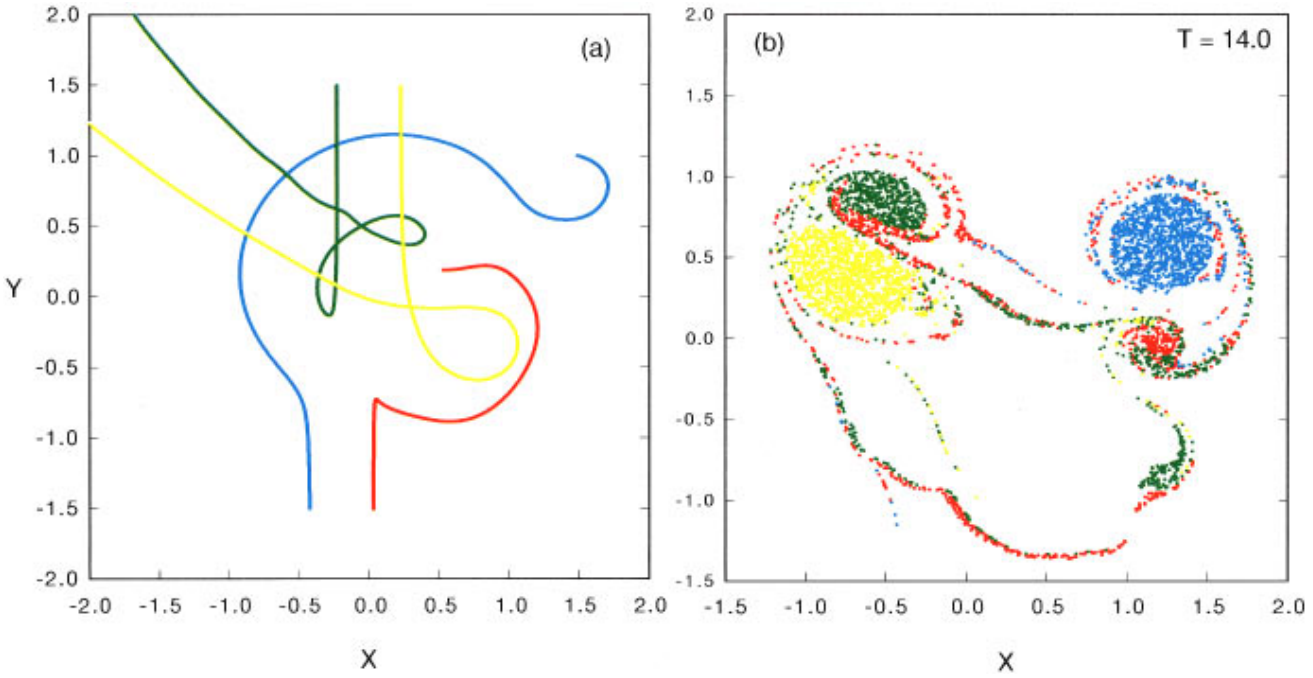

FIG. 7. (Color.) Same as Fig. 5, but for a finite impact parameter $b=0.4$. Only the initial position x_1 of the red-blue dipole has been changed to $x_1=-0.2$. The red orbit is drawn only for $T\leqslant 11.$, i.e., until the second collision in which the red pole is almost completely destroyed.

increases even further. For $b=0.4$ this means that only the stronger of the two dipoles reforms, while for $b=0.6$ the impact parameter at the reforming collision has increased so much that none of the dipoles reforms but only the newly formed green-blue, unbalanced dipole survives. The weaker, red pole of the two dipole halves directly opposite to each other, however, having already lost about half its original fluid in the first collision is completely destroyed in the second collision. This finally leaves its current partner (yellow) effectively as a monopole. With still larger impact parameter, $b=0.8$, the first collision no longer leads to a splitting of the original dipoles. Instead, the dipole halves directly opposite each other (red-green) are strongly deformed and practically slip past each other. In the process, however, the

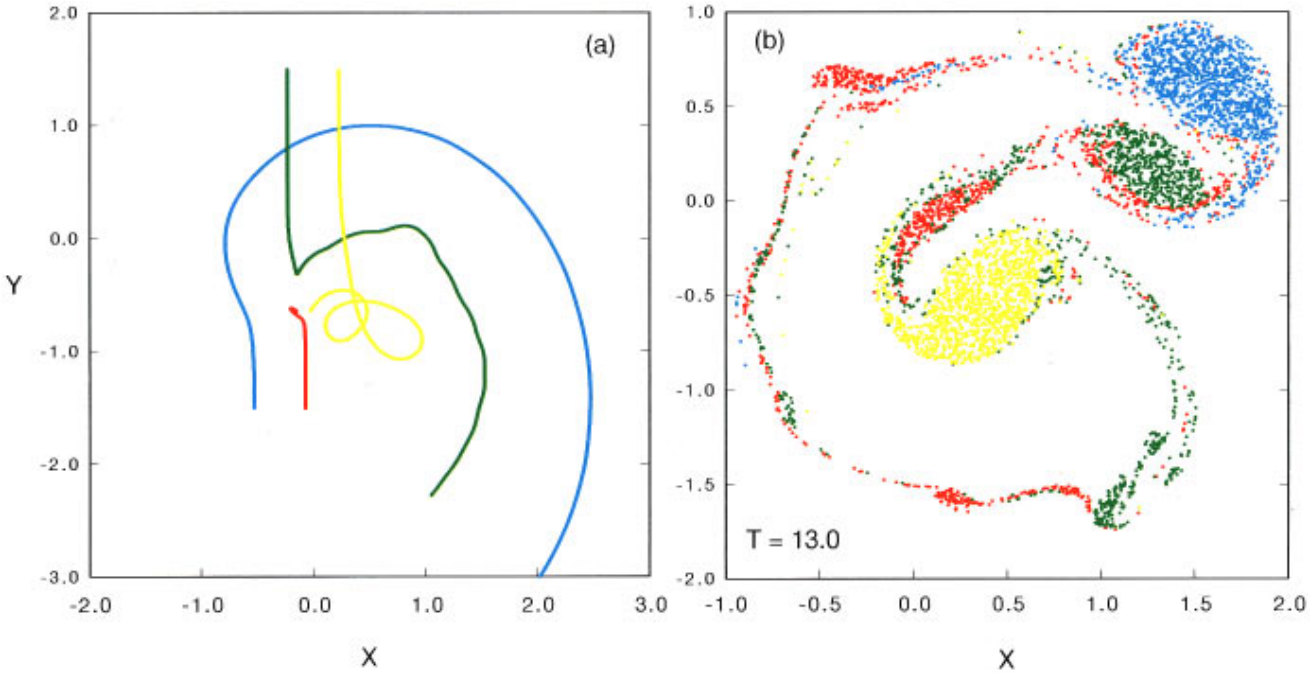

FIG. 8. (Color.) Same as Fig. 5, but for a finite impact parameter $b=0.6$. Only the initial position x_1 of the red-blue dipole has been changed to $x_1=-0.3$. The red orbit is drawn only for $T\leqslant 5.0$, i.e., until just after the first collision when the red pole already has lost about half of its trapped fluid.

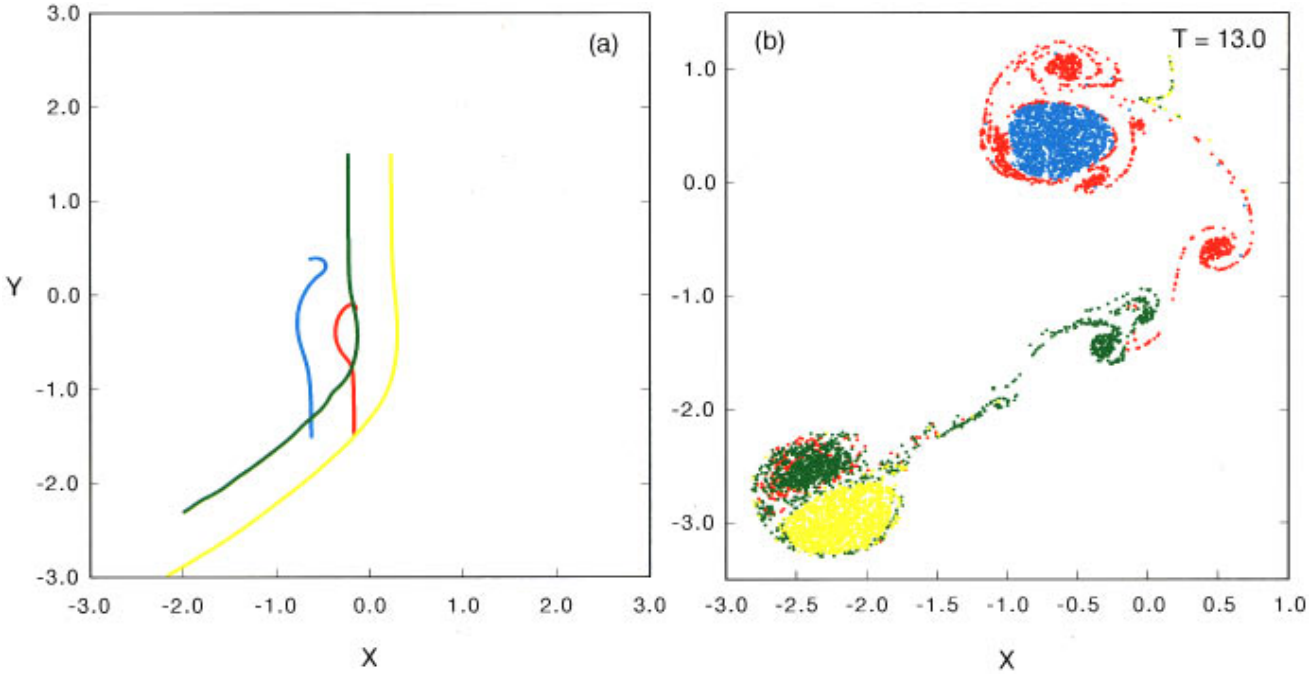

FIG. 9. (Color.) Same as Fig. 5, but for a finite impact parameter $b=0.8$. Only the initial position x_1 of the red-blue dipole has been changed to $x_1=-0.4$. The red orbit is drawn only for $T\leqslant 6.0$.

weaker, red pole is almost completely destroyed. The surviving green-yellow dipole, which has negative velocity, emerges with a large tilt of its axis and will be subject to the tilt instability. A sizable fraction of the fluid lost from the colliding poles is seen to form a number of small monopoles in the wake of the collision. For $b=1.0$, both dipoles slip past each other and emerge with their axes tilted, but both remain largely intact. Again, the negative velocity, yellow-green dipole will then be subject to the tilt instability.

The effect of the collision on the different dipole halves can again be quantified by the loss of fluid from each at the end of the collision process. These results are summarized in Table I. Obviously, the green and red poles directly opposite each other in the finite impact parameter collisions are af-

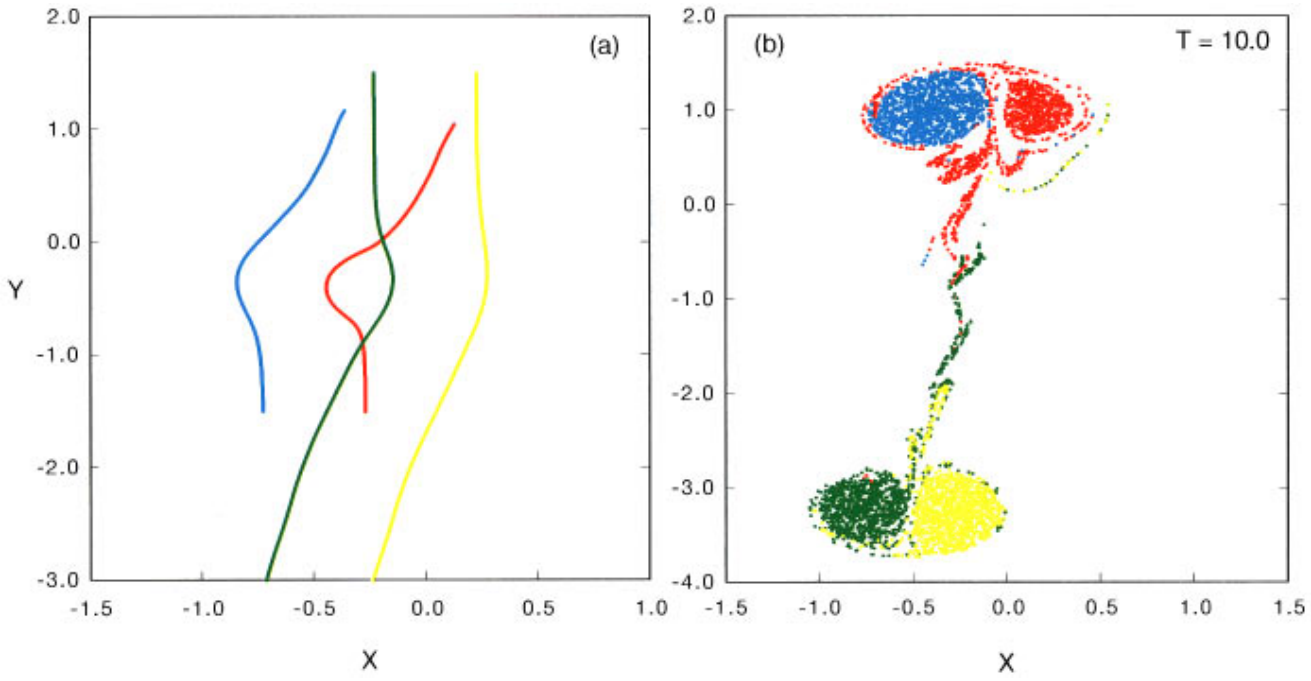

FIG. 10. (Color.) Same as Fig. 5, but for a finite impact parameter $b=1.0$. Only the initial position x_1 of the red-blue dipole has been changed to $x_1=-0.5$.

TABLE I. Fluid and generalized potential vorticity losses (in %) from the various dipole halves after a collision. The values given apply to the same time as the final states depicted in Figs. 5 to 10. Red and blue refer to the positive and negative poles of the downward moving dipole $u=-0.3$, and green and yellow to the positive and negative poles of the upward moving dipole $u=+0.5$. NB: all losses to the yellow pole in the case of $b=1.0$ occur well after the collision as a consequence of the unstable dipole that results from the collision.

Impact parameter		Red	Blue	Green	Yellow
$b=0.0$	Fluid	25	25	14	14
	$\overline{\omega}$	4.2	4.2	1.3	1.3
$b=0.2$	Fluid	35	11	29	10
	$\overline{\omega}$	11	0.9	7.1	0.9
$b=0.4$	Fluid	77	4.0	51	7.2
	$\overline{\omega}$	70	0.4	27	0.5
$b=0.6$	Fluid	76	3.2	58	2.0
	$\overline{\omega}$	53	0.1	28	0.0
$b=0.8$	Fluid	80	0.9	36	2.1
	$\overline{\omega}$	72	0.0	21	0.0
$b=1.0$	Fluid	23	0.4	21	8.6
	$\overline{\omega}$	13	0.0	6.1	1.2

fected most strongly with the effect being strongest for the weaker, red pole, which in some cases has completely disintegrated. Further, it is found that for $b=0.8$ the generalized potential vorticity that is lost from the stronger, green pole is almost completely compensated by the vorticity captured from the red pole.

IV. SUMMARY AND CONCLUSIONS

Particle-in-cell calculations of perturbed and colliding dipole vortices in the Hasegawa-Mima-Charney equation (1) have been performed. An advantage of these PIC calculations is the straightforward possibility to visualize and to quantify the fluid and particle losses, trapping, or mixing between the various vorticity poles themselves and between the poles and the ambient medium.

The fluid and vorticity losses from dipoles perturbed by a finite tilt of their axes is initially seen to occur in bursts. These losses in combination with a mixing of fluid from both poles and a small increase in the separation of the poles are responsible for the damping of the tilt oscillation on the stable branch ($u>0$). As the net vorticity losses are not symmetric between the two dipole halves, the orbit of the dipole on the unstable branch ($u<-v_*$) is changed dramatically: instead of the expected cycloidal orbit, the net velocity along y is completely reversed, leading to a damped oscillatory motion similar to a dipole on the stable branch. Total fluid losses are on the order of 10's of percent in both cases. These losses correspond to a much lower percentage of lost ''generalized potential vorticity'' $\overline{\omega}$, as a consequence of the strong concentration of vorticity near the centers of the poles for the parameters studied.

A dipole collision for parameters identical to those in Ref. [8] has been calculated. In spite of the solitonlike character of the collision, a considerable amount of trapped fluid is seen to be lost from the dipoles (up to 25% for the weaker, red-blue of the two). In addition collisions have been calculated for varying (nonzero) impact parameter. Different values of the impact parameter have large and different consequences. One finds subsequently: $b=0.0$ (Fig. 5): solitonlike; $b=0.2$ (Fig. 6): almost solitonlike, but the asymmetric initial condition leads to a finite tilt of the axes of the reformed dipoles that leaves the yellow-green dipole subject to the tilt instability; $b=0.4$ (Fig. 7): now only the stronger, yellow-green dipole reforms, but not without large losses from the green pole. Of the weaker dipole, the red pole is almost completely torn apart, leaving the blue as a monopole; $b=0.6$ (Fig. 8): reforming no longer occurs in the second collision, instead, while one dipole (green-blue) formed in the first collision survives, the yellow pole survives as a monopole and the red pole is destroyed; $b=0.8$ (Fig. 9): the dipoles no longer split at the collision, but rather slip past each other; in the process the weaker red pole is almost destroyed, while the yellow-green dipole is strongly perturbed obtaining a large tilt; $b=1.0$ (Fig. 10): the dipoles again slip past each other, but now both survive the collision. Note that in most of the cases merging and mixing of like-signed vorticity fluid is mostly limited to fluid that is shed by the dipoles or to the very edges of the dipole halves themselves. Only in the case of $b=0.8$ is a significant merging of red fluid well into the green pole visible, which compensates almost half of the fluid losses from the green pole, while the vorticity losses are compensated almost completely. This case is very similar to the inelastic dipole collision discussed in Ref. [25]. In any case the mixing is limited to the outer regions of the green pole.

As vortices appear to form natural constituents in turbulent flows, they may contribute significantly to transport. Here, especially transport along x, i.e., in the direction of the equilibrium gradient, is of interest. Clearly, a finite tilt of the dipole will play an important role in that case: part of the fluid is transported over distances much larger than the size of the dipole. The precise behavior of dipoles is difficult to predict as relatively modest changes to the dipole, such as a small tilt of its axis and the effect of nearby dipoles, may

have large consequences for its orbit and its integrity. Elastic dipole collisions appear to be the exception rather than the rule (at least for nonzero impact parameter of order 1 or smaller), which limits the lifetime of individual dipoles. All this makes the behavior of dipole vortices in turbulence highly unpredictable. In a turbulent medium vortices might be continuously created and destroyed.

ACKNOWLEDGMENTS

The authors gratefully acknowledge discussions with Professor G. J. F. van Heijst. This work was performed under the Euratom–FOM Association agreement with financial support from NWO and Euratom.

[1] W.H. Matthaeus, W.T. Stribling, D. Martinez, S. Oughton, and D. Montgomery, Phys. Rev. Lett. **66**, 2731 (1991).
[2] H. Brands, J. Stulemeyer, R.A. Pasmanter, and T.J. Schep Phys. Fluids (to be published).
[3] C. Ferro Fontán and A. Verga, Phys. Rev. E **52**, 6717 (1995).
[4] T. Dudok de Wit, S. Benkadda, P. Gabbai, and A.D. Verga, Phys. Rev. E **52**, 6753 (1995).
[5] A. Hasegawa and K. Mima, Phys. Fluids **21**, 87 (1978).
[6] W. Horton and A. Hasegawa, Chaos **4**, 227 (1994).
[7] V.D. Larichev, G.M. Reznik, Oceanology **16**, 547 (1976).
[8] M. Makino, T. Kamimura, and T. Taniuti, J. Phys. Soc. Jpn. **50**, 980 (1981).
[9] J.C. McWilliams, G.R. Flierl, V.D. Larichev, and G.M. Reznik, Dyn. Atmos. Oceans **5**, 219 (1981).
[10] J.C. McWilliams and N.J. Zabusky, Geophys. Astrophys. Fluid Dynamics **19**, 207 (1982).
[11] V.D. Larichev and G.M. Reznik, Oceanology **23**, 545 (1983).
[12] G.G. Sutyrin, J.S. Hesthaven, J.P. Lynov, and J.J. Rasmussen, J. Fluid Mech. **268**, 103 (1994).
[13] C. Ferro Fontán and A. Verga, Phys. Rev. E **52**, 6717 (1995).
[14] J.P. Christiansen, J. Comput. Phys. **13**, 363 (1973).
[15] R.W. Hockney and J.W. Eastwood, *Computer Simulation using Particles* (IOP Publishing, Bristol, 1988).
[16] J. Nycander and M.B. Isichenko, Phys. Fluids B **2**, 2042 (1990).
[17] J.S. Hesthaven, J.P. Lynov, and J. Nycander, Phys. Fluids A **5**, 622 (1993).
[18] J.J. Monaghan, Comput. Phys. Rep. **3**, 73 (1985).
[19] W.H. Press, S.A. Teukolsky, W.T. Vetterling, and B.P. Flannery, *Numerical Recipes in FORTRAN*, 2nd ed. (Cambridge University Press, Cambridge, 1992).
[20] W. Arter and J.W. Eastwood, J. Comput. Phys. **117**, 194 (1995).
[21] J.D. Meiss and W. Horton, Phys. Fluids **26**, 990 (1983).
[22] J. Nycander, Phys. Fluids A **4**, 467 (1992).
[23] M. Kono and W. Horton, Phys. Fluids B **3**, 3255 (1991).
[24] O.U. Velasco Fuentes and G.J.F. van Heijst, J. Fluid Mech. **259**, 79 (1994).
[25] W. Horton, Phys. Fluids B **1**, 524 (1989).